TÜBİTAK

Turkish Journal of Biology

http://journals.tubitak.gov.tr/biology/

Research Article

Turk J Biol
(2016) 40: 380-398
© TÜBİTAK
doi:10.3906/biy-1502-49

Collagen/PEO/gold nanofibrous matrices for skin tissue engineering

Ömer AKTÜRK[1], Dilek KESKİN[1,2,*]

[1]Department of Engineering Sciences, Middle East Technical University, Ankara, Turkey

[2]BIOMATEN, Center of Excellence in Biomaterials and Tissue Engineering, Middle East Technical University, Ankara, Turkey

Received: 18.02.2015 • **Accepted/Published Online:** 19.05.2015 • **Final Version:** 23.02.2016

Abstract: As a novel approach in skin tissue engineering, gold nanoparticles (AuNPs) were synthesized and incorporated at different concentrations into collagen/PEO nanofibrous matrices in this study. The group containing 14.27 ppm AuNPs (CM-Au) had the best nanofibrous morphology. CM-Au was cross-linked with glutaraldehyde vapor (CM-AuX). All groups were disrupted in collagenase in 2 h, but cross-linked groups and Matriderm® resisted hydrolytic degradation for 7 and 14 days, respectively. Due to its small pores and dense structure, lower water swelling results (7.26 ± 2.62 g/g) were obtained for CM-AuX than Matriderm (17.51 ± 1.97 g/g). CM-Au and Matriderm had statistically similar tensile strength and elastic modulus, but elongation at break of CM-Au (over 100%) was significantly better than that of Matriderm. After cross-linking, tensile strength and elastic modulus of collagen matrix was further improved. AuNPs (37 and 42 nm) seemed to be nontoxic on 3T3 fibroblasts and keratinocytes for different time periods. CM-AuX scaffold extracts were also nontoxic for 3T3 fibroblasts and keratinocytes. The L929 cell attachment and proliferation on CM-AuX were comparable with Matriderm, indicating good in vitro biocompatibility. As a whole, collagen matrices incorporated with AuNPs are potential biomaterial candidates for skin tissue engineering.

Key words: Nanofibrous matrix, electrospinning, collagen, gold nanoparticles

1. Introduction

The use of collagen in development of a biomaterial is a common route due to its well-known outstanding biocompatibility features, low toxicity to most tissues, and well-documented structural, physical, chemical, and immunological properties (Duan and Sheardown, 2006). Although it possesses all these desirable properties, collagen is mechanically weak in its purified state and shows fast degradation in aqueous environments. Therefore, biological or synthetic cross-linking agents such as genipin, glutaraldehyde, N-(3-dimethylaminopropyl)-N-ethyl-carbodiimide hydrochloride (EDC), and EDC with N-hydroxy-sulfosuccinimide have been widely used as collagen cross-linking agents to increase the stability with a high degree of mechanical integrity (Huang and Shanmugasundaram, 2015).

Electrospinning of collagen nanofibers is very popular in tissue engineering and regenerative medicine because they can mimic the biochemical and ultrastructural properties of the native extracellular matrix (ECM) of tissues. Therefore, many studies have focused on developing electrospun scaffolds from collagen only or their blends with natural or synthetic polymers for different tissue engineering applications. Electrospun collagen scaffolds have long been shown to be promising candidates for skin tissue engineering applications in particular (Buttafoco et al., 2006; Rho et al., 2006; Chen et al., 2008; Hsu et al., 2010; Lin et al., 2013). There are also recent publications related to the wound healing (Lee et al., 2015) and skin regeneration (Zhou et al., 2015) effects of collagen-based nanofibrous scaffolds.

These above-mentioned properties of electrospun collagen fibers could still be improved by incorporating functional additives such as gold nanoparticles, which have important benefits from the perspective of tissue engineering applications. For instance, they have been shown to improve scaffolds due to their unique properties such as enhanced mechanical stability and resistance against enzymatic degradation (Deeken et al., 2011; Grant et al., 2014), easy incorporation of antibodies (Obaid et al., 2015), growth factors (Paviolo et al., 2015), and peptides (Gopalakrishnan et al., 2015) by their immobilization at the gold surface, enhanced biocompatibility (Cui et al 2014; Grant et al., 2014; Hung et al., 2014), and possible antioxidant (Sanna et al., 2014; Balasubramani et al., 2015) and antimicrobial (Li et al., 2014; Regiel-Futyra et al., 2015; Ehmann et al., 2015) behavior.

* Correspondence: dkeskin@metu.edu.tr

Hence, these important properties could make them promising candidates in tissue engineering applications such as vascular (Hung et al., 2014), cardiac (Ravichandran et al., 2014; Shevach et al., 2014) bone (Ko et al., 2015), and skin (Cozad et al., 2011; Silveira et al., 2014) applications. In addition, gold nanoparticles have already been used in conjugation with electrospun fibers in a series of studies related to tissue engineering applications. For example, a collagen/hyaluronic acid polymer blend conjugated with gold nanoparticles was electrospun into a scaffold material for the treatment of osteoporosis (Fischer et al., 2012). Nanocomposite scaffold integrating coiled electrospun fibers with gold nanoparticles was also reported for cardiac tissue engineering (Fleischer et al., 2014). Polymethylglutarimide nanofibers functionalized by grafted AuNPs, which were labeled with cell-adhesive peptides, enhanced HeLa cell attachment and potentiated cardiomyocyte differentiation of human pluripotent stem cells (Jung et al., 2012).

In this study, considering all the reported data, we develop a nanofibrous collagen matrix incorporating AuNPs for potential skin tissue engineering applications. To our knowledge, there is no study to date on the preparation and characterization of scaffolds of collagen/PEO nanofibers incorporated with gold nanoparticles for skin tissue engineering applications. It is proposed in the current study that the advantageous properties of collagen nanofibrous matrix, such as similar nanofibrous structure to skin and the proven wound healing effect reported in the literature, could be enhanced by incorporating AuNPs into the collagen matrix due to the above-mentioned unique properties of AuNPs. Such scaffolds are expected to create a suitable surface for host cell attachment and proliferation or provide a source of collagen with high surface area due to their nanofibrous structure. The nanofibrous structure will likely increase the absorption of cell adhesion proteins and so will attract the cells to the wound bed without infection or inflammation (potential antibacterial and antioxidant effect of AuNPs), thereby improving the healing rate of the wounded skin tissue.

2. Materials and methods

2.1. Materials

Collagen from bovine Achilles tendon (powder), acetic acid (ReagentPlus, ≥99%), glutaraldehyde solution (GTA, 25%), poly(ethylene oxide) (PEO, M_v ~4,000,000), collagenase from *Clostridium histolyticum* (Type I-A, lyophilized powder), ethylene diamine tetraacetic acid disodium salt dihydrate (EDTA, 99%), thiazolyl blue tetrazolium bromide (MTT bromide, approx. 98% TLC), trypan blue solution (0.4%), and trisodium citrate dihydrate ($Na_3C_6H_5O_7{\cdot}2H_2$) were obtained from Sigma Aldrich (Germany). Glycine (electrophoresis purity reagent) was obtained from Bio-Rad Laboratories (USA). Hydrogen tetrachloroaurate(III) ($HAuCl_4{\cdot}3H_2O$) and dimethyl sulfoxide (DMSO, cell culture grade, min. 99.5%) were obtained from AppliChem (Germany). Millex syringe filter units (disposable, Durapore, 0.1 µm, PVDF) were obtained from Merck Millipore (Germany). Formvar carbon film-coated (200 mesh) copper grids for transmission electron microscopy (TEM) were bought from Electron Microscopy Sciences (USA). All the cell culture solutions and reagents were purchased from Merck Millipore (Germany), unless otherwise stated in the text.

2.2. Methods

2.2.1. Synthesis of gold nanoparticles

Gold nanoparticles were synthesized with the citrate reduction method, also known as the Turkevich method (Kimling et al., 2006). $HAuCl_4{\cdot}3H_2O$ (1 g) was dissolved in distilled water to get 1 mM gold salt solution (solution I). Solution I (20 mL) was stirred with a magnetic stirrer while heating. While stirring at high speed (800 rpm), previously prepared 1% trisodium citrate dihydrate ($Na_3C_6H_5O_7{\cdot}2H_2$) solution (solution II) was added at different volumes (7–10 mL) to boiling solution I for AuNPs synthesis. When the color of the solution started to turn from pale blue (nucleation) to deep red (ruby red), the stirring at the boiling point was continued for another 15 min. Immediately after this step, the flask containing the solution was soaked in an ice bath to stop the reaction. Finally, the AuNP suspension was topped to 30 mL and passed through a 0.1-µm filter to get the stock AuNP solution (157 ppm). The synthesized AuNPs were labelled as Au7, Au8, Au9, and Au10 according to the citrate volume added.

2.2.2. Characterization of gold nanoparticles

High contrast TEM analysis was done using an FEI Tecnai G^2 Spirit BioTwin operating at 120 kV to evaluate the size and shape of AuNPs in the central laboratory of Middle East Technical University (METU). Before the analysis, AuNP suspensions were subjected to sonication and vortexing processes to prevent agglomeration and aggregation. AuNP suspensions were dripped onto carbon-coated copper grids, which were then dried in an oven. AuNP size distribution analysis was performed using the Image J program on three different TEM images of all groups, each containing at least 100 nanoparticles.

2.2.3. Fabrication of nanofibrous matrices

Collagen nanofibrous matrices were obtained by electrospinning of collagen/PEO blend solutions. In the preparation of nanofibrous scaffolds, the flow rate of the collagen solutions dripping out of the blunt needle (18 G) of syringes was adjusted to 0.8 mL/h with a syringe pump (New Era, USA) and they were collected on a stationary circular aluminum collector disc (D = 5 cm) located 23

cm away from the syringe needle. The voltage of the high-voltage power supply (Gamma, USA) connected to the needle tip was adjusted to 19 kV. The nanofibrous matrices were peeled off from the collectors and stored in a desiccator until tests. The effect of AuNPs on the electrospinning of collagen/PEO blend solutions was examined by adding different amounts of AuNPs into the blends (Table 1). The collagen solution (1%, 10 mL) dissolved in acetic acid (0.5 M) having 2% or 2.5% PEO were added with different volumes of AuNPs from the stock AuNP solution (157 ppm) to get different concentrations of AuNPs in the blends. The total polymer blend concentration was fixed (2.73% or 3.18%). AuNP dispersion inside the nanofibers was examined by TEM in the central laboratory of METU. TEM samples were prepared by collecting AuNP-loaded nanofibers on carbon-coated copper grids.

Since the electrospun matrices were observed to lose their structural integrity to a large extent in aqueous environments, they were cross-linked with GTA vapor (3%) for different time periods (2 and 4 h) at room temperature. Unreacted aldehyde groups were blocked in glycine solution (0.2 M) for 30 min after GTA cross-linking before in vitro biocompatibility tests. Graded ethanol series (20%–100%) were used for dehydration or rehydration of scaffolds.

2.2.4. Physicochemical characterization of nanofibrous matrices

2.2.4.1. Scanning electron microscopy

Electrospun matrices were sputter-coated with gold-palladium (E1010, Ion Sputter, Hitachi, Japan) before analysis by scanning electron microscopy (SEM; S-3000H, Hitachi, Japan) at the Department of Metallurgical and Materials Engineering of METU. For each scaffold, three random micrographs were taken and diameters of at least 100 randomly selected fibers from each micrograph were measured using the Image J program. Fiber diameter and the distribution of fiber sizes of each scaffold were averaged from at least 300 fibers.

2.2.4.2. Attenuated total reflectance Fourier transform infrared spectrophotometer analysis

Infrared spectra were measured with an attenuated total reflectance Fourier transform infrared (ATR-FTIR; IFS/66S, Hyperion 1000) spectrophotometer in the central laboratory of METU. Each spectrum was acquired in transmittance mode on a ZnSe ATR crystal cell by accumulation of 256 scans with a resolution of 4 cm^{-1} and a spectral range of 4000–400 cm^{-1}.

2.2.4.3. Hydrolytic and enzymatic degradation

The degradation of scaffolds (CM-Au14, CM-Au14X, and Matriderm®) in an aqueous environment was analyzed. The samples, cut to 1 × 1 cm^2, were put into PBS (pH 7.2, 0.01 M) and incubated at 37 °C until the integrity of their structures was disrupted. In vitro degradation of the scaffolds was also performed by incubating the scaffolds in PBS solution (pH 7.2, 0.01 M, 5 mL) containing 60 µL of type I collagenase solution (1 mg/mL). The mass loss of collagen from the scaffolds was measured by gravimetric analysis. Gravimetrical analysis was carried out by removing the scaffolds at the specified incubation periods (1, 4, 7, and 14 days) and measuring their weights after complete drying with lyophilization to get the % degradation results using the following equation (n = 4):

$$\text{Degradation (\%)} = \frac{W_d - W_t}{W_d} \times 100 \ . \quad (1)$$

W_d denotes the initial dry weight of the test samples, while W_t represents the dry degraded weight at each incubation time.

Table 1. The composition of electrospinning groups.

Groups	Collagen conc. in final sol. (% w/v)	PEO conc. in final sol. (% w/v)	Blend ratio, C:PEO (w/w)	Total blend conc. (% w/v)	AuNPs conc. in final sol. (ppm)
Col1Au0	1	-	1:0	1	0.14
Col2Au0	2	-	2:0	2	0.14
Col1P2Au0	0.91	1.8	1:2	2.73	0.14
Col1P2Au1	0.91	1.8	1:2	2.73	1.42
Col1P2.5Au0	0.91	2.27	1:2.5	3.18	0.14
Col1P2.5Au1	0.91	2.27	1:2.5	3.18	1.42
Col1P2.5Au7	0.91	2.27	1:2.5	3.18	7.13
Col1P2.5Au14	0.91	2.27	1:2.5	3.18	14.27

2.2.4.4. Equilibrium degree of swelling

Equilibrium water content of collagen matrices (CM-Au, CM-AuX) and Matriderm was measured by a general gravimetric method. Scaffolds from each group were cut into 1 × 1 cm^2 pieces and their dry weights (W_d) were measured. Each sample was immersed in PBS at 37 °C. All bottles were capped tightly and water inside the bottles was removed daily. After removal of excess surface water by gently blotting with a filter paper, the PBS-equilibrated swollen weights of the scaffolds were measured (W_s). Finally, equilibrium degree of swelling (EDS) was calculated using the following equation (n = 4):

$$EDS = \frac{W_s - W_d}{W_d} \times 100 \ . \quad (2)$$

2.2.4.5. Mechanical tests

The mechanical properties of collagen matrices (CM-Au, CM-AuX) and Matriderm were evaluated by applying a stretch test with the Lloyd LS500 Material Testing Machine (Lloyd, UK) using Nexygen computer software. Rectangular samples (5 × 30 mm) were cut from scaffolds. To prevent slippage from the grips, they were covered with sand paper at the attachment site. The gauge length and width were 10 and 5 mm, respectively. The thickness of the test samples were measured by vernier caliper and found to be about 0.3–0.5 mm for collagen nanofibrous matrices and 1 mm for Matriderm. The crosshead speed of the system was adjusted to 10 mm/min to get a constant strain rate of 100%/min. The results of tests were obtained as load versus deflection curves, which were then converted into stress-strain data by the computer program. Ultimate tensile strength (UTS), percent elongation at break (EAB), and modulus of elasticity (E) were calculated from the stress-strain curves (n ≥ 6).

2.2.5. In vitro biocompatibility tests

2.2.5.1. Cell culture conditions

The HaCat human keratinocyte (DSMZ, Germany), 3T3 fibroblast (An1 Swiss albino mouse fibroblast, Foot-and-Mouth Disease Institute of the Ministry of Agriculture and Rural Affairs of Turkey), and L929 mouse fibroblast (ATCC, USA) cell lines were cultured in complete cell culture medium, i.e. Dulbecco's modified Eagle's medium (DMEM, high glucose-glutamine) supplemented with fetal bovine serum (FBS, 10%, v/v) and penicillin/streptomycin (10 U/mL) at 37 °C under humidified atmosphere of 5% CO_2 and 95% air in an incubator (5215, SHEL LAB, USA). When the cells reached at least 80%–90% confluency, they were trypsinized with trypsin/EDTA solution (0.1% in PBS) and counted with a cell counter (Nucleocounter, LI-COR, USA).

2.2.5.2. Cytotoxicity tests of synthesized AuNPs

Keratinocytes and 3T3 fibroblasts were seeded onto 12-well plates at the seeding density of 100 cells/μL (30,000 cells/well). After a 1-day incubation period, AuNPs were added to cell-seeded 12-well plates at different concentrations (10 and 20 ppm). The desired nanoparticle concentration was achieved by diluting the stock AuNP suspension (157 ppm) with complete cell culturing medium. Complete cell culturing medium without AuNPs was used as the control. The stock AuNP suspension was previously sterilized by passing it through a sterile 0.1-μm filter. The cytotoxic effect of Au7 and Au8 was evaluated with MTT cell viability assay for different incubation time periods (1, 4, and 7 days). Medium containing AuNPs was refreshed every other day for longer incubations. Briefly, MTT stock solution (5 mg/mL) was prepared by dissolving it in PBS buffer. The MTT test solution was prepared by diluting this stock in a 1/10 ratio with DMEM (without phenol red). At the end of each time period, the medium was removed and washed with PBS. Subsequently, 500 μL of MTT test solution was added to each well. The test wells were incubated at 37 °C in a dark environment for 4 h. Afterwards, MTT test solution was removed and 500 μL of DMSO was added, and wells were shaken at 200 rpm for 15 min. Spectrophotometric measurements were done at 550 nm wavelength (n = 4). The cell viability (%) was also calculated by normalizing the OD results to control.

2.2.5.3. Cytotoxicity tests of scaffold extracts

The cytotoxicity test of CM-AuX extract was performed according to modified ISO 10993-5 and ISO 10993-12 standards. Briefly, CM-AuX was initially exposed to UV light for 30 min and then held in 70% ethanol supplemented with antibiotics (penicillin/streptomycin, 10 U/mL) overnight for sterilization. After sterilization, the samples were rinsed with distilled water completely and held in DMEM temporarily. They were then incubated in extract medium (DMEM) at 37 °C for different time periods (1, 4, and 7 days) while shaking at 200 rpm. DMEM without any scaffolds was used as the control. Keratinocytes or 3T3 fibroblasts were seeded onto 12-well plates at the seeding density of 100 cells/μL (30,000 cells/well) and, after 1 day of seeding, the medium was removed and refreshed with extract medium of different time periods and supplemented with FBS (10%). After 1 day, cell viability was evaluated with MTT assay as mentioned previously. In summary, the medium was removed and washed with PBS. Subsequently, 500 μL of MTT test solution was added to each well. The test wells were incubated at 37 °C in a dark environment for 4 h. Afterwards, MTT test solution was removed and 500 μL of DMSO was added, and wells were shaken at 200 rpm for 15 min. Spectrophotometric measurements were done at 550 nm wavelength (n = 3). The cell viability (%) was also calculated by normalizing the OD results to the control.

2.2.5.4. Cell attachment and proliferation on scaffolds

The sterilized scaffolds (CM-AuX and Matriderm) were cut into rectangular shapes (1 × 1 cm) and put onto sterile 24-well suspension plates. Before the cell seeding, the samples were kept in DMEM briefly. Afterwards, L929 fibroblasts were seeded onto scaffolds at a seeding density of 100 cells/μL (100,000 cells/well) and held in a CO_2 incubator for 1 and 3 days. The cell culture medium inside the wells was refreshed every other day. Eventually, the medium was removed and the scaffolds seeded with cells were fixed in 3% GTA (in PB) solution for 1 h at room temperature. They were completely dehydrated in a lyophilizator and then they were coated with gold and analyzed by SEM (JSM-6400 Electron Microscope, JEOL Ltd., Japan) at the Department of Metallurgical and Materials Engineering of METU.

2.2.6. Statistical analysis

In comparing the groups for a single parameter, one-way analysis of variance (ANOVA) was done with Tukey's multiple comparison test for the post hoc pairwise comparisons using SPSS 22 (IBM Corp., USA). Differences were considered significant at $P < 0.05$.

3. Results

3.1. Characterization of AuNPs

AuNPs having sizes of 28–42 nm were synthesized in the experiments (Figure 1). According to TEM results, meaningful differences were not encountered with the amount of sodium citrate added, except for the Au10 group. Nevertheless, when the citrate was increased, the size distribution and uniformity of shape of the AuNPs were enhanced clearly. Different AuNPs shapes (rectangular, triangular, or rod-like) other than spherical particles were observed more pronouncedly for lower volumes of citrate (Au7). After this volume, the spherical particles in the AuNPs solutions were dominant (Au8, Au9, and Au10). The shape and size distribution of the Au8 and Au9 groups were very similar. The Au10 group also had AuNPs smaller than 20 nm, which was supposed to have a potential to cause toxicity according to preliminary cytotoxicity tests (data not shown). As a consequence, Au8 was decided to be the most appropriate group to be used in electrospinning solutions.

3.2. Physicochemical characterization of collagen matrices

3.2.1. Incorporation of AuNPs into matrices

During the optimization studies of electrospinning it was found that the best results were achieved with operating parameters of 0.8 mL/h flow rate, 23 cm distance between tip and collector, and 19 kV voltage. In the first step, by changing these parameters, a continuous outflow from the syringe was achieved to obtain fibrous structures on the collectors. In the second step, further optimizations were done to improve the morphological and structural properties of the formed fibrous matrices in terms of obtaining nanoscale, uniform fibers and defect-free nanofibrous structures. The results of optimization studies were analyzed by visual observations and SEM analysis (data not shown).

After defining these operating parameters, one of the AuNP groups (Au8) having highly monodisperse size distribution and uniform shape was selected to be added into collagen/PEO blend solutions for electrospinning. As a result, nanofiber accumulation on the collector was achieved (Table 2). The spinnability of collagen-only solutions supplemented with AuNPs was also checked before electrospinning experiments of blend solutions. As expected, no fibers but only beads were obtained in these groups. In collagen/PEO blend groups to which different amounts (0.14, 1.42, 7.13, 14.27 ppm) of AuNPs were added, nanofibrous matrices were obtained. The most successful matrices were obtained in the groups having a collagen/PEO ratio of 1:2.5. According to our observations, increasing the collagen concentration from 1% to 2% resulted in an unexpected increase in viscosity. Consequently, this prevented the continuous and uniform fiber jet outflow from the syringe tip during electrospinning process. Hence, 1% collagen concentration was selected to be the most appropriate concentration for electrospinning. The increase in the amount of AuNPs added to collagen/PEO solutions enhanced the morphology and size distribution of nanofibers. Fibrous intact structure with perfect morphology was observed visually for the collagen/PEO blend group containing 14.27 ppm AuNPs. The appearance of AuNPs inside the nanofibers of collagen/PEO blends was viewed with TEM (Figure 2). Identification of the AuNPs inside the nanofibers was very difficult at lower concentrations of AuNPs (0.14 and 1.42 ppm). However, detecting the AuNPs in the nanofibers became much easier in the groups supplemented with greater amounts of AuNPs (7.13 and 14.27 ppm).

3.2.2. Morphology of nanofibrous matrices

SEM analysis (Figure 3) indicated that in collagen matrices (Col1P2Au0 and Col1P2Au1) fabricated from a solution of collagen/PEO at a ratio of 1:2, micron-sized film-like structures (droplet shapes) formed abundantly on the fibers independent of AuNP amount added. For collagen matrices (Col1P2.5Au0, Col1P2.5Au1, Col1P2.5Au7, and Col1P2.5Au14) obtained from solutions of collagen/PEO at a ratio of 1:2.5, these droplet shapes were observed again (Figure 4). The increase in the amount of AuNPs in the spinning solutions obviously enhanced the morphology of nanofibers such that these microdroplets gradually disappeared and smoother and defect-free nanofibers were obtained. Among the electrospun groups, the

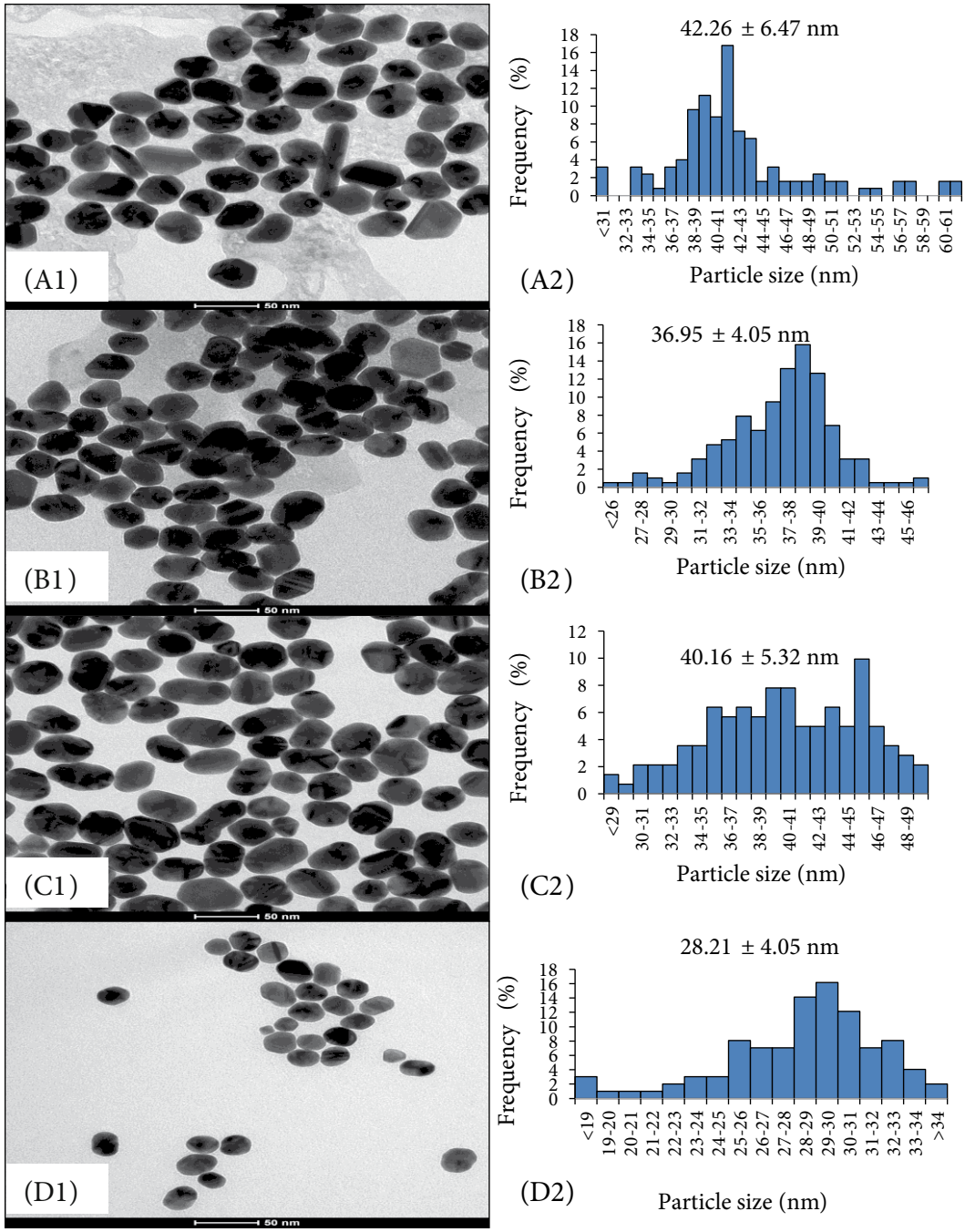

Figure 1. TEM micrographs and size distribution histograms of synthesized different AuNPs groups: **A1–A2)** Au7, **B1–B2)** Au8, **C1–C2)** Au9, and **D1–D2)** Au10.

collagen matrix containing the maximum amount of AuNPs (Col1P2.5Au14) was decided to have excellent fiber morphology (very uniform fiber size distribution and no structural deformations) and was therefore selected for further physicochemical characterization tests. This group was labeled as CM-Au. It was failed to fabricate control nanofibrous matrix groups without AuNPs. As shown in Figures 3 and 4, related to scaffold morphologies, scaffolds containing the least amount of AuNPs had too many deformities. The situation for collagen/PEO scaffolds without any AuNPs was even worse. Therefore, the scaffolds containing the minimum amount of AuNPs (0.14 ppm) were used as controls to justify the use of AuNPs.

Nanofibrous structure of the Col1P2.5Au14 group (CM-Au) was protected to a great extent after the cross-linking treatment with GTA vapor (3%) for 2 and 4 h

Table 2. The results of electrospinning experiments.

Groups*	The properties of the structure accumulated on the collector
Col1Au0	Only liquid droplets
Col2Au0	Only liquid droplets
Col1P2Au0	Fibrous structure, but many morphological deformities such as liquid droplets and beads
Col1P2Au1	Fibrous structure, but many morphological deformities such as liquid droplets and beads
Col1P2.5Au0	Fibrous structure, but many morphological deformities such as liquid droplets and beads
Col1P2.5Au1	Fibrous structure with few morphological deformities
Col1P2.5Au7	Fibrous intact structure with few morphological deformities
Col1P2.5Au14	Fibrous intact structure with perfect morphology

*The compositions of electrospinning groups are given in Table 1.

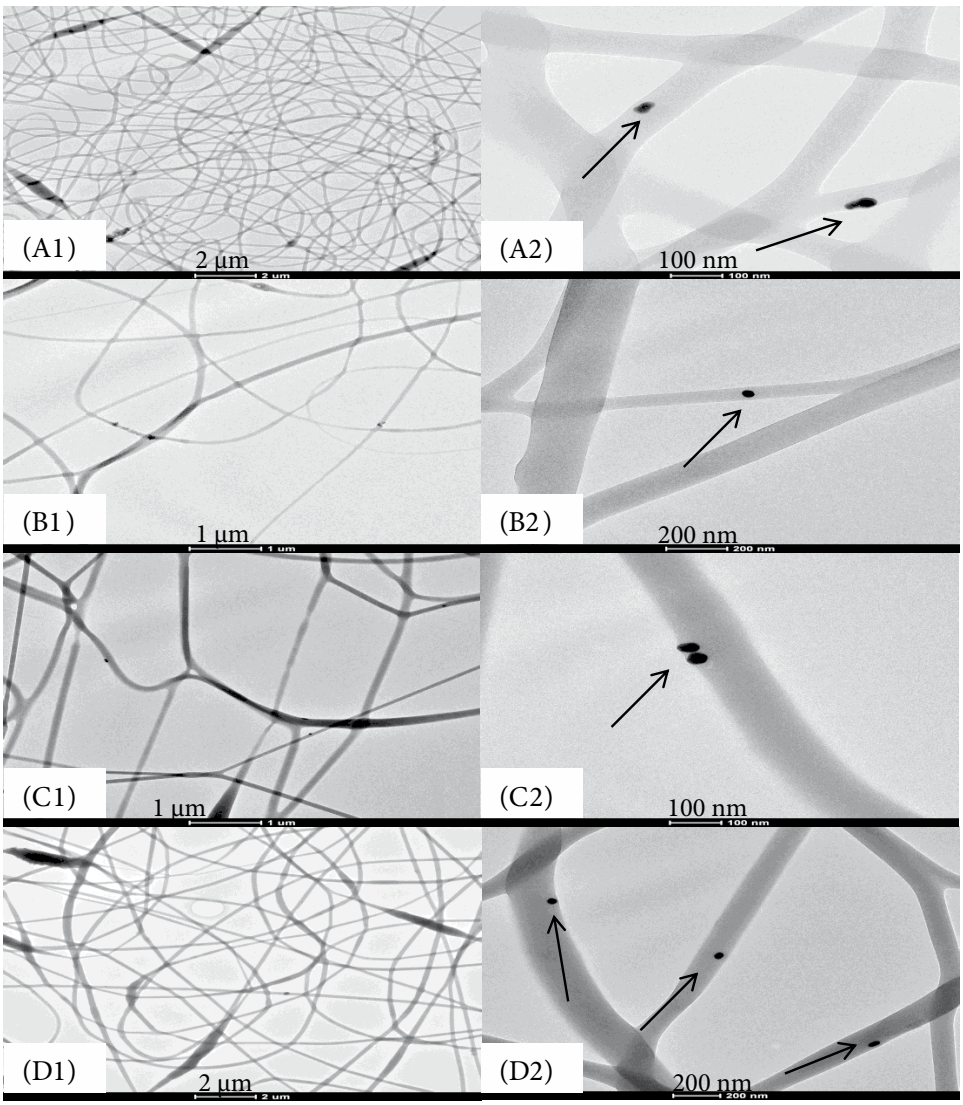

Figure 2. TEM micrographs showing the distribution of AuNPs inside the nanofibers of different matrices: **A1–A2)** P2.5Col1Au0, **B1–B2)** P2.5Col1Au1, **C1–C2)** P2.5Col1Au7, and **D1–D2)** P2.5Col1Au14 groups. Arrows indicate AuNPs.

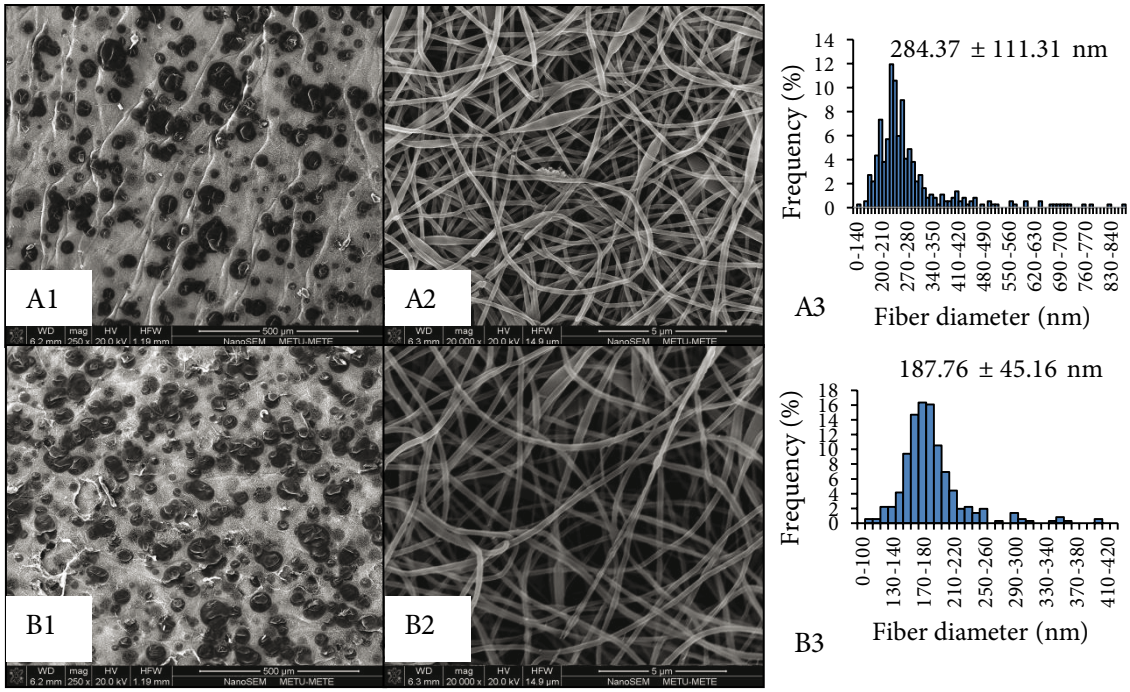

Figure 3. SEM micrographs showing the fiber morphology and fiber diameter distribution of different matrices: **A1–A3)** Col1P2Au0 and **B1–B3)** Col1P2Au1 group.

(Figure 5). The pore size range of CM-Au cross-linked for 2 or 4 h was between 0.5 and 3 μm. However, with increase in cross-linking duration (4 h), a considerable decrease was observed in the pore structure of CM-Au matrices and nearly nonporous regions were formed on them. Furthermore, the immediate degradation behavior of the uncross-linked collagen matrix in an aqueous environment was prevented sufficiently with 2 h of GTA cross-linking. Hence, 2 h of cross-linking treatment duration was decided to be convenient. The Col1P2.5Au14 group cross-linked for 2 h was labeled as CM-AuX.

3.2.3. FTIR analysis of collagen nanofibrous matrices

Before the other characterization tests, the selected groups (CM-Au and CM-AuX) and their matrix constituents (PEO and collagen type I) were characterized by FTIR spectroscopic analysis. The infrared-active modes of the peptide backbone are expressed in the amide bands. Characteristic absorption bands of collagen are located at about 1640 cm^{-1}, 1540 cm^{-1}, and 1250 cm^{-1}, which represent the amide I, II, and III bands of collagen (Sionkowska and Kozłowska, 2010). The main amide characteristic absorption bands of collagen type I and collagen matrices were observed at 1630–1651 cm^{-1} (amide I), 1538–1544 cm^{-1} (amide II), and 1235–1240 cm^{-1} (amide III), as shown in Figure 6. The absorption bands at 2500–3300 cm^{-1} are the O–H stretching contribution of collagen. The region from 970 cm^{-1} to 1200 cm^{-1} is also distinct in collagen, with the highest absorption bands observed at 1060 cm^{-1} (collagen type I), 1098 cm^{-1} (CM-Au), and 1097 cm^{-1} (CM-AuX), generally ascribed to C–O vibrations of alcohols, either from hydroxyproline or from the glycosidic side chain of collagen (Chang and Tanaka, 2002). The absorptions at 839 cm^{-1}, 944 cm^{-1}, and 959 cm^{-1} (=CH2 bending); 1090 cm^{-1}, 1240 cm^{-1}, and 1278 cm^{-1} (O–C stretching); 1359 cm^{-1} and 1466 cm^{-1} (O–H bending); and 2859 cm^{-1} (O–H stretching) were clearly observed for PEO. After the conjugation with AuNPs and GTA cross-linking, visual inspection of the spectrum revealed that these characteristic bands were conserved.

3.2.4. Hydrolytic and enzymatic degradation of matrices

CM-Au degraded immediately in PBS at 37 °C, whereas after cross-linking (CM-AuX) it had a high first-day hydrolytic degradation (HD) result (85%), which slowed down in the following days, and the structural stability of the remaining scaffold was maintained for 7 days (Figure 7). HD of Matriderm was much slower than that of CM-AuX with only a little degradation (20%) at the first day. Matriderm could maintain its structural integrity for 2 weeks. The resistance of all test groups (CM-Au, CM-AuX, and Matriderm) against enzymatic degradation (ED) was very weak since they all degraded completely in 1 day. As a whole, the cross-linking treatment increased the resistance of collagen-based scaffolds against HD only, but the resistance against ED was not improved under the testing conditions.

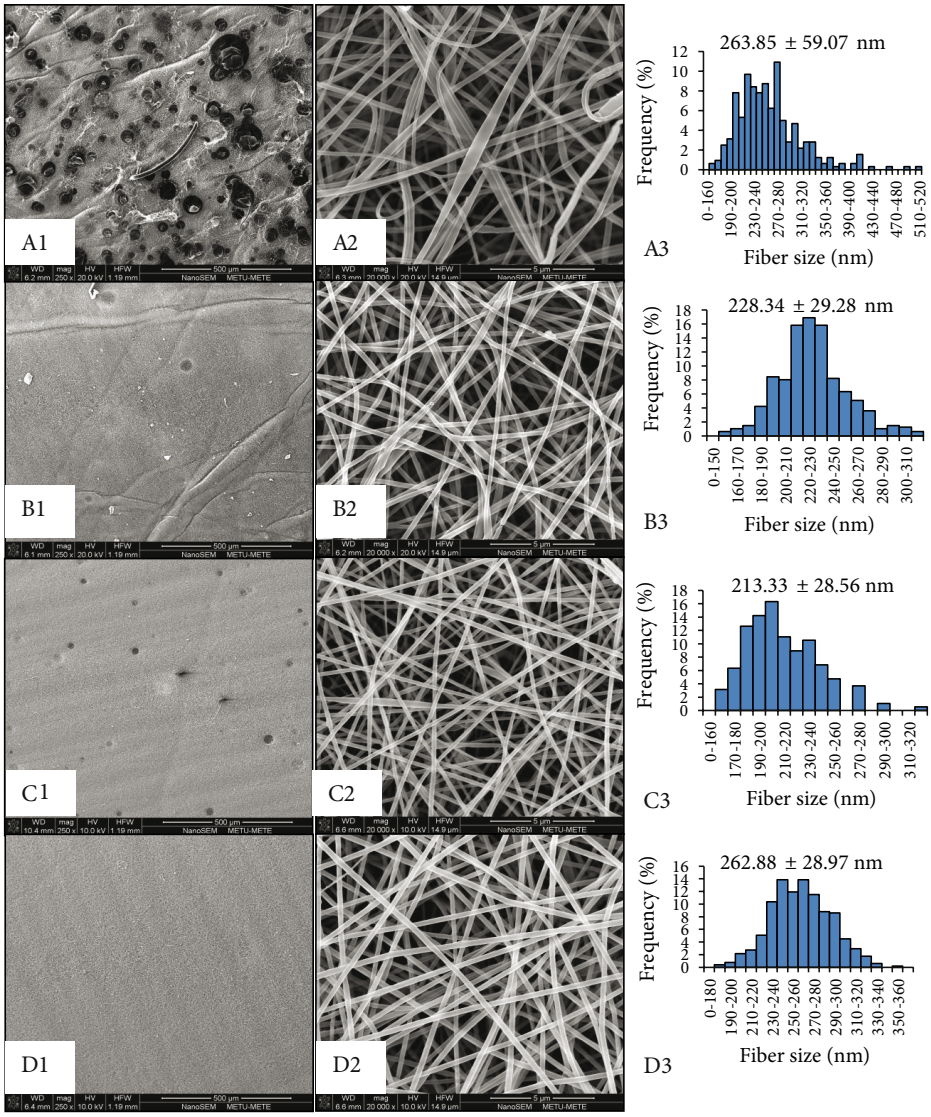

Figure 4. SEM micrographs showing the fiber morphology and fiber diameter distribution of different matrices: **A1–A3)** Col1P2.5Au0, **B1–B3)** Col1P2.5Au1, **C1–C3)** Col1P2.5Au7, **D1–D3)** Col1P2.5Au14.

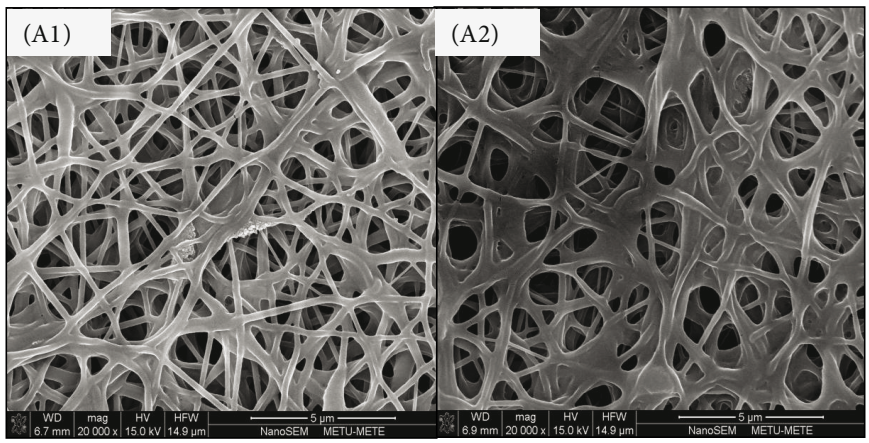

Figure 5. SEM micrographs showing the change in nanofiber morphology and pore size of CM-Au after cross-linking with GTA vapor (3%) for different time periods: **A1)** 2 h and **A2)** 4 h.

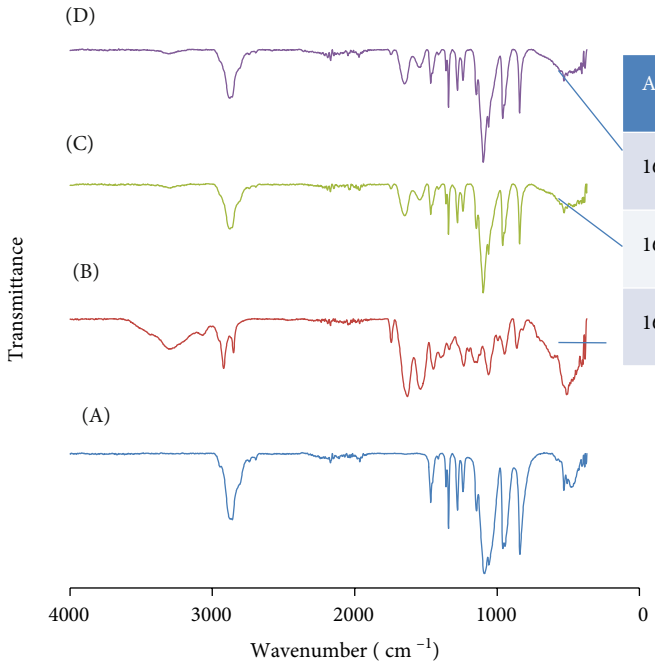

Amide I	Amide II	Amide III
1650.96	1541.48	1240.17
1649.32	1544.33	1240.39
1629.79	1538.39	1234.51

Figure 6. FTIR-ATR spectra of test groups: **A)** PEO, **B)** collagen type I, **C)** CM-Au, and **D)** CM-AuX.

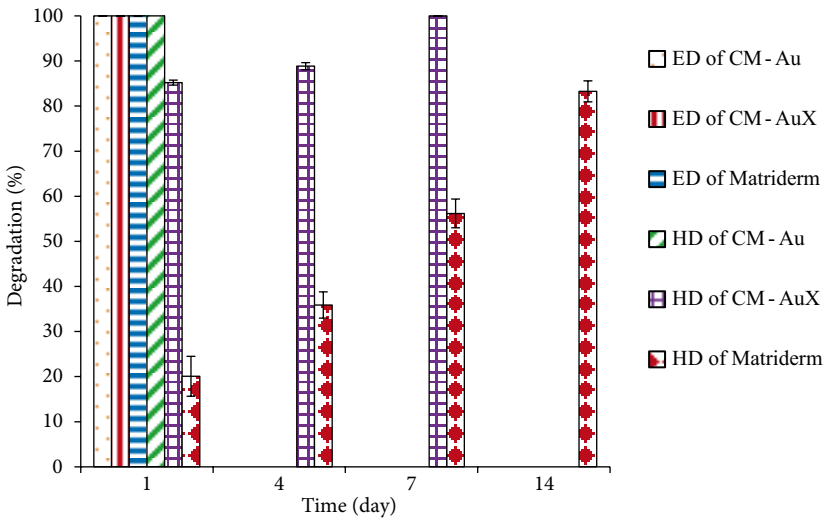

Figure 7. Hydrolytic (HD) and enzymatic (ED) degradation results of collagen matrices (CM-Au and CM-AuX) and Matriderm.

3.2.5. Equilibrium degree of swelling of scaffolds

The EDS value (7.26 ± 2.62 g/g) of CM-AuX was not very high. This was probably due to the fact that CM-AuX contained small pores and had a dense film-like structure as shown in previous results. EDS of CM-AuX was significantly lower than that of Matriderm (17.51 ± 1.97 g/g), which has a spongy and porous structure increasing the water swelling capacity.

3.2.6. Mechanical tests

The representative stress-strain curves of CM-Au, CM-AuX, and Matriderm are given in Figure 8A. The elastic region for CM-Au was very small with low yield stress (about 0.1 MPa). After cross-linking, this linear region became very distinct with higher yield stress values (0.2–0.4 MPa). Collagen nanofibrous matrices had a long nonlinear plastic region that became smaller after cross-linking. On

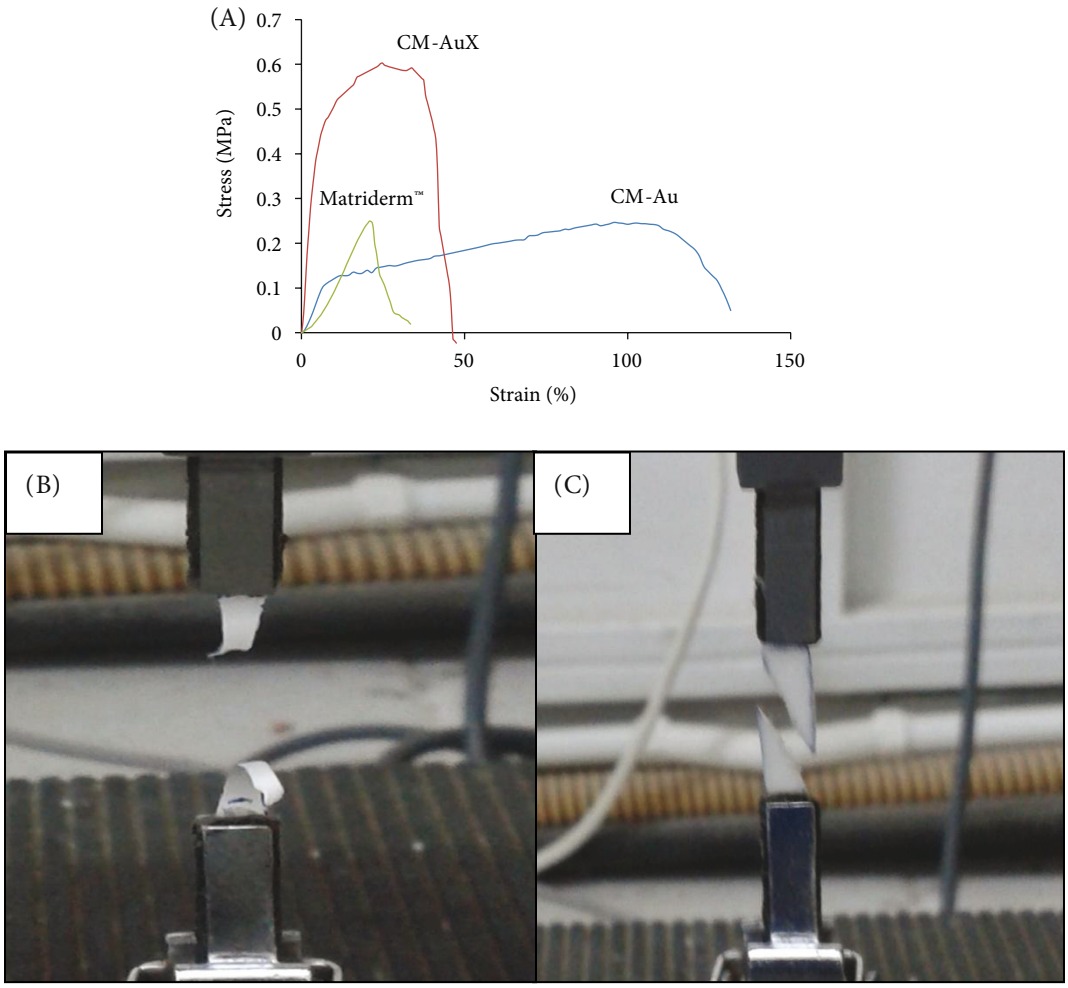

Figure 8. A) Representative stress-strain curves of collagen matrices and Matriderm and the photos demonstrating the successful tensile break of **B)** collagen matrices and **C)** Matriderm.

the other hand, the plastic region of Matriderm was barely realized or completely lost, showing a brittle material behavior in dry test conditions. Due to the delicate nature of the groups tested, only the tensile breaks occurring in the middle of the gauge length were accepted as successful (Figures 8B and 8C) and included in the statistical analysis to discard the false results.

The results of the test groups (CM-Au, CM-AuX, and Matriderm) are compared in Table 3. Mechanical properties of CM-Au were statistically similar to Matriderm except for EAB value. CM-Au could elongate more than 100%, which was statistically higher than the other groups. However, after cross-linking, the EAB of CM-Au became statistically similar to the EAB of Matriderm. As opposed

Table 3. Mechanical properties of collagen matrices and Matriderm.

Groups	UTS (MPa)	EAB (%)	E (MPa)
CM-Au	0.29 ± 0.031^{b}	106.90 ± 14.97^{bc}	1.82 ± 0.38^{b}
CM-AuX	0.53 ± 0.079^{ac}	28.64 ± 4.23^{a}	6.38 ± 1.96^{ac}
Matriderm®	0.33 ± 0.077^{b}	22.41 ± 2.55^{a}	1.67 ± 0.31^{b}

Data are expressed as mean ± SD ($n \geq 6$). [a] Significant difference from CM-Au for $P < 0.05$. [b] Significant difference from CM-AuX for $P < 0.05$. [c] Significant difference from Matriderm for $P < 0.05$.

to the decrease of EAB, UTS and E values of CM-AuX increased such that these values of CM-AuX became statistically higher than those of the other groups.

3.3. In vitro biocompatibility tests

3.3.1. Cytotoxicity tests of AuNPs

Cytotoxicity tests were carried out for Au7 and Au8 on keratinocytes and 3T3 fibroblasts. Dose (10 and 20 ppm) and time (1, 4, and 7 days) effects of AuNP cytotoxicity on these cells were investigated as well. According to day 1 results, there was no significant difference between different doses of Au7 and Au8 groups and the control group for keratinocytes (Figures 9A and 9B), but significant differences between different doses of Au7 and Au8 groups and the control group were observed for 3T3 fibroblasts (Figures 9C and 9D). Keratinocyte cell viabilities were 98%–88% for Au7 and 90%–92% for Au8 at day 1. On the other hand, fibroblast cell viabilities were 67%–70% for Au7 and 68%–72% for Au8 at day 1. These results verified that these doses (10 and 20 ppm) of Au7 and Au8 were noncytotoxic to keratinocytes but slightly cytotoxic to fibroblast in a 1-day period.

After 4 days, there were significant differences between dose groups of Au7 and Au8 and the control for both cell types, except for the OD of the 10 ppm dose of Au7 for fibroblasts (Figures 9A–9D). While keratinocyte cell viability results were 65%–73% for Au7 and 87%–88% for Au8 at day 4, fibroblast cell viabilities were 85%–91% for Au7 and 79%–82% for Au8 at day 4. According to these

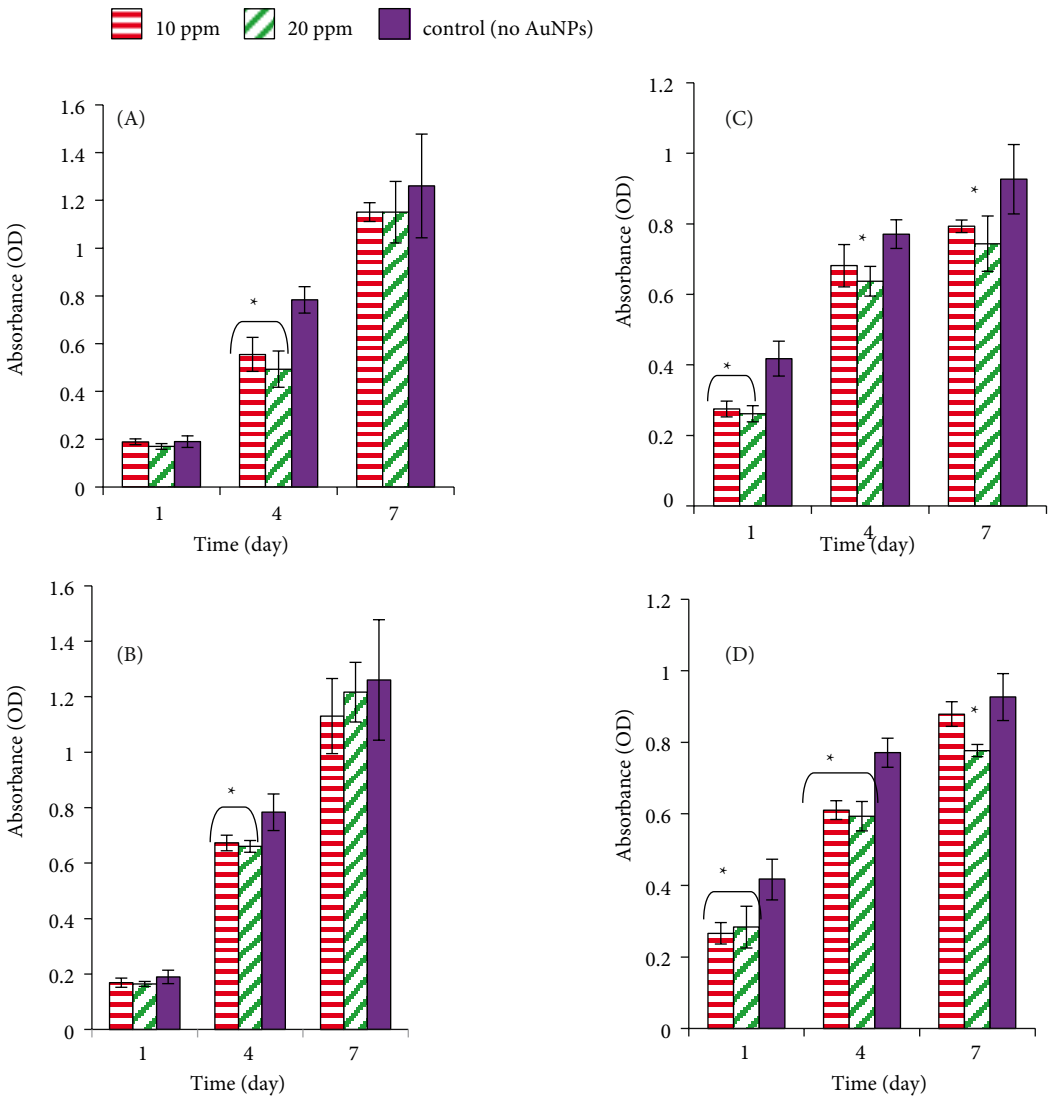

Figure 9. Cytotoxicity tests of different AuNPs groups: **A)** Au7 and **B)** Au8 on keratinocytes and **C)** Au7 and **D)** Au8 on 3T3 fibroblasts with MTT assay. *: Indicates a significant difference from the control in the same time period (n = 6 ± SD, $P < 0.05$).

results, the defined doses of Au8 were noncytotoxic to keratinocytes and fibroblasts, but a slight cytotoxic effect of Au7 was observed on keratinocytes at 4 days. In addition, no statistically meaningful difference occurred among the doses of Au7 and Au8 at day 4 for both cell types.

According to the OD results measured after an incubation period of 7 days, the OD results in all of the AuNP groups were statistically similar to the control for both cell types, except for the OD values of the 20 ppm dose group of both Au7 and Au8 for fibroblasts (Figures 9A–9D). Keratinocyte cell viabilities were 91% for Au7 and 90%–97% for Au8 at day 7. On the other hand, fibroblast cell viabilities were 80%–86% for Au7 and 84%–95% for Au8 at day 7. These results verified that the defined doses of Au7 or Au8 were noncytotoxic to keratinocytes and fibroblasts at 7 days. Between each time period, the cells proliferated significantly for all of the doses of Au7 and Au8.

3.3.2. Cytotoxicity tests of scaffold extracts

After determining the noncytotoxic size/shape and dose level of AuNPs and using these data to load potentially safe AuNPs into matrices, their extracts were also characterized for the verification of nontoxicity. Reduction of cell viability by more than 30% is considered a cytotoxic effect according to ISO 10993-5 standards. The cell viability of CM-AuX changed between 88% and 99% for HaCat keratinocytes (Figure 10A) and 76% and 96% for 3T3 fibroblasts (Figure 10B) for different time periods (1, 4, and 7 days). According to these results, the extracts of CM-AuX were decided to be nontoxic for all of these time periods.

3.3.3. Cell adhesion and proliferation studies

Performing cytotoxicity tests on synthesized AuNPs and collagen matrix extracts was still not sufficient to assess the biocompatibility of matrices and their corresponding safe use as a scaffold material for skin tissue engineering. Therefore, together with these tests, cell attachment and proliferation on collagen matrices were evaluated. It is known that cell attachment and proliferation are crucial for a skin substitute to support and guide new tissue formation. SEM micrographs revealed that after 1 day of incubation time, L929 fibroblasts adhered on CM-AuX and Matriderm tightly with typical spindle-like morphology spreading over the scaffold surface (Figures 11A and 11B). Stretching of cell pseudopods was not so clear for any of the groups and globular cytoskeleton cell structure was detected more easily. Cellular proliferation was also observed to increase on both the collagen matrices and Matriderm during the 3-day incubation period (Figures 11C and 11D). The extensive cell proliferation on CM-AuX was comparable to Matriderm. This result proved that the CM-AuX fabricated in this study preserves the original good cytocompatibility of collagen.

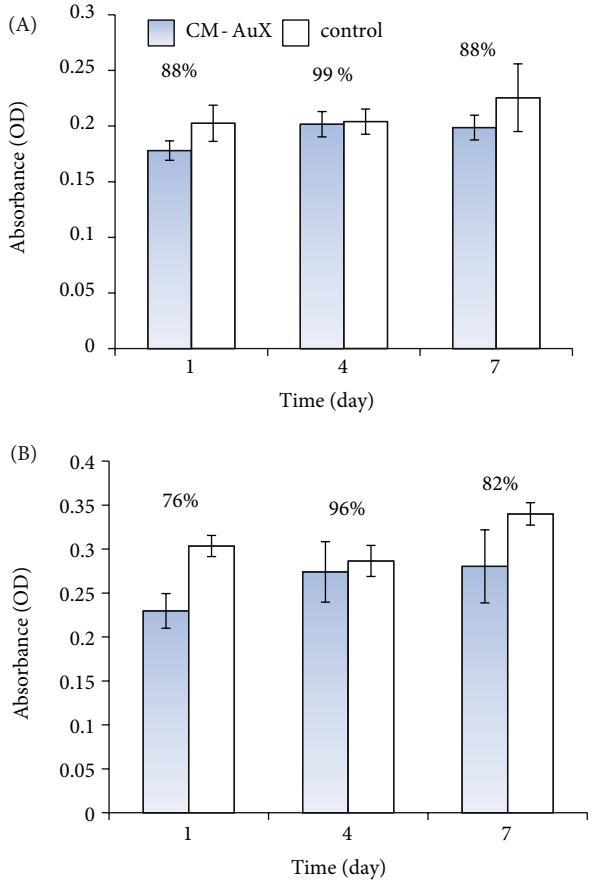

Figure 10. Extract cytotoxicity tests of CM-AuX on **A)** keratinocytes and **B)** 3T3 fibroblasts in different time periods (n = 3 ± SD).

4. Discussion

The chemical synthesis of AuNPs by citrate reduction of the corresponding gold salt is an apparently simple process, which only requires the mixing of the gold salt and sodium citrate at well-defined concentrations and external conditions such as temperature, pH, and stirring rates. As shown in the study of Kimling et al. (2006), these conditions can affect the final morphology of the particles. In the present study, the gold salt concentration and the external conditions were kept constant and the amount of sodium citrate in the reaction solution was changed. As Frens (1973) pointed out, the variation of the citrate concentration modifies the gold particle size within a large interval. The explanation for this effect is the role that citrate plays in the passivation of formed gold particles. A high citrate concentration allows the stabilization of smaller particles, while for smaller concentrations, the coverage is incomplete and a coarsening process leads to the aggregation of larger entities. Similar to our study, spherical-shaped and monodisperse AuNPs with the size range of 10–30 nm were obtained in different studies using

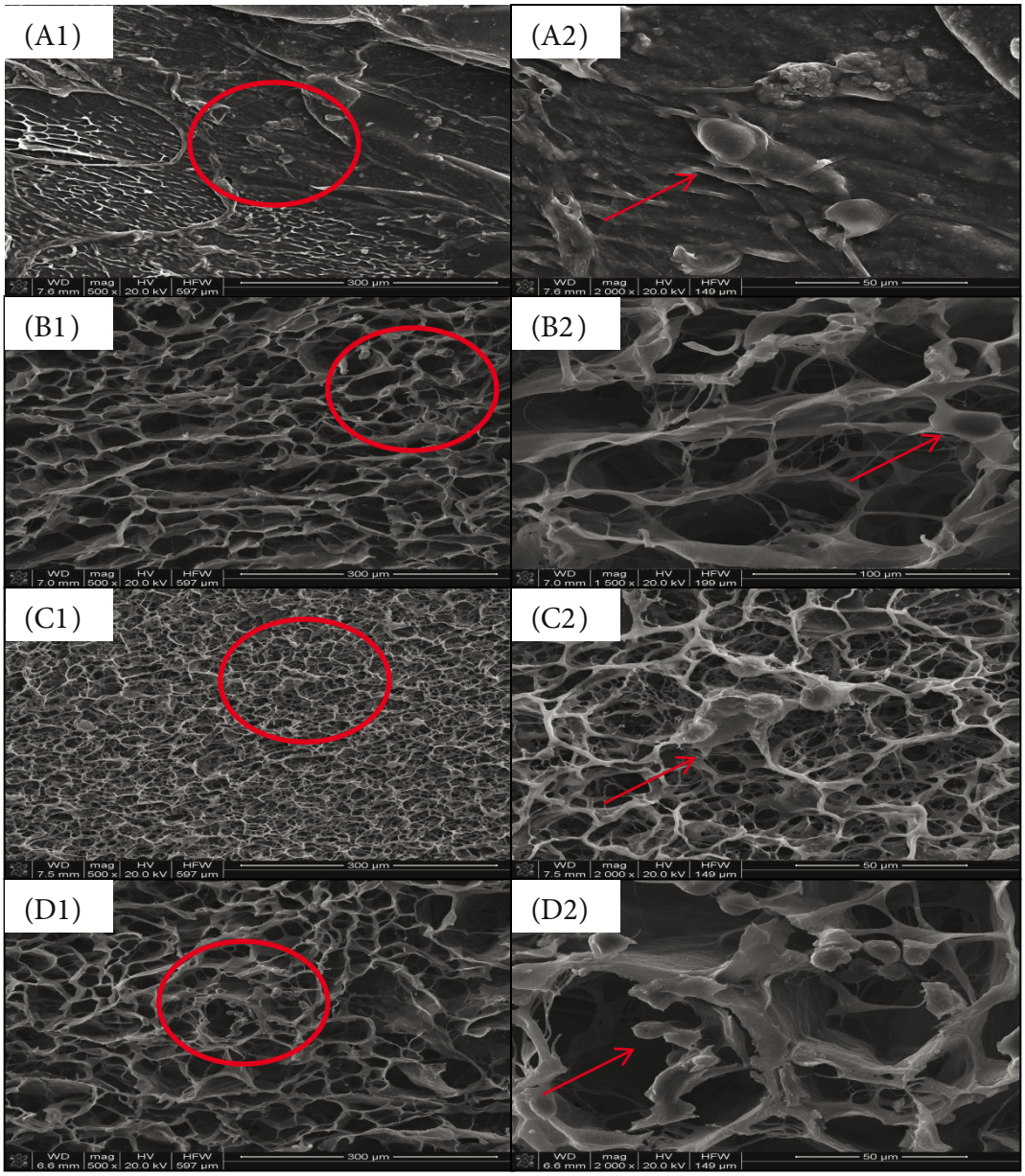

Figure 11. SEM micrographs showing the adhesion of L929 fibroblasts in 1-day incubation period on **A1–A2)** CM-AuX and **B1–B2)** Matriderm and the proliferation of L929 fibroblasts in 3-day incubation period on **C1–C2)** CM-AuX and **D1-D2)** Matriderm. Red circles and arrows indicate cells.

the Turkevich method (Zhou et al., 2012; Agarwal et al., 2015; Schlinkert et al., 2015). Nanoparticles were shown to have a tendency to aggregate and precipitate subsequently (Zhou et al., 2012; Agarwal et al., 2015). In this study, this common problem was tried to be solved by applying sonication and vortexing the stock AuNPs before the tests. When the original red color, a clear indication of AuNPs, shifted to blue, this was accepted as a sign of aggregation of AuNPs. The AuNPs synthesized in this study had absorbance at 500–600 nm (data not shown) as a result of the excitation of surface plasmons, which shift to longer wavelengths when aggregates form. Addition of AuNPs into collagen solutions caused no visible changes in color, so it was supposed that the stability of AuNP suspensions was conserved adequately.

In the initial electrospinning experiments, it was not possible to obtain nanofibrous scaffolds from pure collagen solutions in the experimental conditions of this study. Similarly, Huang et al. (2001) failed to prepare continuous collagen fibers from collagen-only solutions, so they used PEO to aid in the electrospinning process. Here, a green synthesis method based on dissolving

collagen type I in weak acid (0.5 M acetic acid solvent) was preferred and therefore no toxic organic solvents were used. Pure collagen solutions can only be electrospun when organic solvents such as HFIP are used (Matthews et al., 2002; Rho et al., 2006). There are some studies that achieved the electrospinning of a special type of collagen (Semed S collagen) dissolved in a mixture of PBS/ethanol (Dong et al., 2009). Electrospinning of collagen in weak acid solutions was always accomplished with the help of PEO as shown by other studies in the literature (Huang et al., 2001; Buttafoco et al., 2006; Chen et al., 2008). In optimization experiments, electrospun matrices obtained from the blends of collagen and PEO were found to have discontinuities such as beads or liquid droplets. After numerous trials, collagen and PEO concentrations in the blends were adjusted to be optimum at 1% and 2.5%, respectively. The collagen nanofibrous matrix selected as the best group in our study had a collagen nanofiber diameter similar to the human ECM (Duan et al., 2013). Collagen nanofiber diameters produced in other studies related to skin tissue engineering were in the range of about 100–500 nm (Rho et al., 2006; Chen et al., 2008; Hsu et al., 2010; Zhou et al., 2015), similar to the nanofiber size range of our study.

Cell migration into the CM-AuX matrix would not be possible since it had a small pore size range (0.5–3 μm). The size range of L929 cells is 5–10 μm (Higuchi and Tsukamoto, 2004). Thus, it might be inferred that average pore sizes of greater than 10 μm are necessary to allow cell passage and migration. On the other hand, it should also be considered that the CM-AuX expands by 2–5 times upon contact with an aqueous environment. In addition, PEO is readily soluble in water and it might act like a porogen during incubation in aqueous cell culture environments. Therefore, although pore size ranges in initial dry conditions might not be suitable for cell migration, larger pores might be formed upon contact with an aqueous environment in time. For instance, silk fibroin scaffolds were observed to have cells dwelling only on the surface of mats when PEO was not extracted, while some cells migrated underneath the silk fibers on PEO-extracted mats (Jin et al., 2004). There are also studies in the literature that used PEO to create a porous environment suitable for cell penetration into the scaffold (Baker et al., 2008; Lowery et al., 2010).

For uncross-linked (CM-Au) and cross-linked (CM-AuX) matrices, each absorption peak of collagen and PEO was identified, which confirms that both collagen nanofibrous matrices were composed of these two polymers. However, the absorption peak of –N=CH– (1622 cm^{-1}), which represents the imide bond formation between aldehyde and amino groups during the cross-linking step, cannot be clearly identified due to interference from the 1649–1651 cm^{-1} (amide I) peak (Chen et al., 2008). The absorption bands at 2500–3300 cm^{-1} are the O–H stretching contribution of collagen. The addition of AuNPs into collagen/PEO matrices caused the disappearance of O–H bands of collagen type I observed at 2500–3300 cm^{-1}, with only a remaining O–H stretching band at about 2900 cm^{-1} that might be attributed to PEO. This suggested that collagen/PEO stabilized AuNPs (Fathi-Azarbayjani et al., 2010). It was also shown that the amide absorption bands of the groups did not change significantly, which was an indication of the undisturbed α-helix secondary structure of collagen, but both cross-linking with GTA and AuNP incorporation shifted the amide I and II absorption bands.

It was aimed with the degradation tests to confirm to what extent the cross-linking treatment influenced the degradation results and to investigate whether the AuNP incorporation would have any contribution on the degradation results. It has already been shown that GTA cross-linking of collagen scaffolds enhanced the resistance against hydrolytic or collagenase degradation (Charulatha and Rajaram, 2003; Wittaya-Areekul and Prahsarn, 2006). There are also studies stating that AuNPs cross-linked to collagen-based scaffolds had enhanced resistance against enzymatic degradation (Castaneda et al., 2008; Deeken et al., 2011; Grant et al., 2014). However, the high hydrolytic and enzymatic degradation results of collagen matrices developed in this study could be due to the ineffectiveness of GTA cross-linking for collagen type I alone. It was stated in a study (Lin et al., 2013) that collagen type I alone could be insufficient for the provision of free $–NH_2$ and the triple-helix structure of collagen might have caused steric hindrance, and all these might have resulted in deterioration of the cross-linking efficiency of GTA. Not only could this low cross-linking efficiency have caused the quick disruption of collagen matrices (CM-AuX) in an enzymatic environment, but the high concentration of the collagenase type I used in this study could also be another reason. For the same reason, Matriderm degraded in this high-concentration enzymatic environment very quickly as well.

The ability of a scaffold to preserve water is an important property for skin tissue engineering. The water-binding ability of the scaffolds could be attributed to their hydrophilicity, their morphology, and the maintenance of their three-dimensional structure. The decrease in dimensions of the scaffold due to contraction or degradation in an aqueous environment also decreases EDS. EDS values obtained in different studies in the literature varied greatly. The EDS value of collagen-chitosan nanofibrous wound dressing scaffolds (Chen et al., 2008) was 3 and 9 g/g for uncross-linked and GTA vapor cross-linked groups, respectively. EDS values of nanofibrous matrices obtained by electrospinning of polylactide–

polyglycolide/collagen blends ranged between 1.8 and 2.2 g/g (Liu et al., 2010). EDS values of nanofibrous matrices obtained by electrospinning of collagen/polyvinyl alcohol/chitosan blends ranged between 0.5 and 2 g/g (Lin et al., 2013). Thus, the EDS values of collagen-based nanofibrous matrices in the literature were similar to the values in this study. As a whole, the EDS values of the prepared scaffolds were thought to be appropriate for skin tissue engineering applications.

The UTS and E values of CM-AuX were slightly lower than or in the range of the reported tensile strength (2.5–16 MPa) and elastic modulus (6–40 MPa) values of human skin (Silver, 1994). There are some variations in the mechanical properties of collagen nanofibers fabricated in different studies, probably due to differences in collagen nanofiber diameter, cross-linking treatment, thickness, etc. For instance, GTA cross-linked collagen nanofibers had 7–11 MPa UTS in dry and wet testing conditions (Rho et al., 2006). Collagen/chitosan nanofibrous wound dressing had 0.5–1 MPa UTS, 0.3–0.7 MPa E, and 2%–23% EAB values (Chen et al., 2008). Electrospun matrices as wound dressing prepared from *Rana chensinensis* skin collagen/poly(L-lactide) mixtures had UTS, EAB, and E values of 0.2–3 MPa, 5%–40%, and 32–38 MPa, respectively (Zhang et al., 2015). Mechanical properties of nanofibrous matrices obtained by electrospinning of collagen/polyvinyl alcohol/chitosan blends were about 1–7 MPa UTS, 5–50 MPa E, and 15–50% EAB (Lin et al., 2013). Electrospun type I collagen/polycaprolactone blends had 0.8–1.9 MPa UTS and 54%–61% EAB (Chakrapani and Gnanamani, 2012). As seen, the mechanical results of CM-AuX were compatible with the literature data. In addition, the mechanical properties of the CM-AuX were comparable to commercial skin substitute (Matriderm). This indicated that CM-AuX would probably provide a similar or even better level of mechanical stability when applied in the wound treatment procedure.

In our study, in order to be able to synthesize potentially biocompatible AuNPs, key parameters such as the size and shape of the nanoparticles were considered at first, because it was shown that cytotoxicity of AuNPs was dependent on the shape, size, dose, and type and charge of surface capping/reducing agents as well as cell type. For instance, it was demonstrated that smaller AuNPs (1.4 nm) were cytotoxic for connective tissue fibroblasts, epithelial cells, and macrophages and melanoma cells, whereas bigger AuNPs in the 15-nm size range were nontoxic even at high concentrations (Pan et al., 2007). The higher surface area to volume ratio of AuNPs might lead to more intense interactions with cellular components and the penetration of smaller-sized AuNPs into intracellular locations like nucleus could be easier, thus causing cytotoxicity (Pan et al., 2007). Gold nanorods have been shown to be more cytotoxic than AuNPs; however, the reason for this was attributed to the coatings, such as cetyltrimethylammonium bromide (Wang et al., 2008). It was suggested that the cationic AuNPs were more cytotoxic than the same-size anionic ones due to the affinity of cationic particles to the negatively charged cell membrane (Goodman et al., 2004). It was also found that citrate-capped AuNPs were not cytotoxic to baby hamster kidney cells and human hepatocellular liver carcinoma cells, but were cytotoxic to human carcinoma cells at certain concentrations (Patra et al., 2007). It was stressed that keratinocyte proliferation was inhibited at doses of AuNPs (34 nm) higher than 10 ppm; on the other hand, lower doses (5 ppm) were shown to enhance the cellular activity for 5 days of incubation (Lu et al., 2010). We also came up with a similar conclusion that toxicity of keratinocytes were dose-dependent for the synthesized AuNPs (37 and 42 nm), but 20 ppm was the toxic dose limit. Slight differences between different studies related to AuNP cytotoxicity are not surprising due to the tendency of AuNPs for aggregation in cell culture media (Wang et al., 2008). It was also demonstrated in our study that bigger AuNPs (37 and 42 nm) appeared not to cause any cytotoxic effect on fibroblasts and keratinocytes, especially at low concentrations (5 and 10 ppm). As a consequence, the AuNPs in these sizes were supposed to have no clear adverse effect on cell proliferation or cell viability of fibroblasts and keratinocytes for short or long time periods. Considering all results, AuNPs groups did not have any cytotoxic effect on the cells during different incubation periods, but it should be noted that as the dose increased, cell viabilities decreased slightly. Fibroblasts seemed to be especially more sensitive to dose increase of these AuNPs sizes. Hence, the fabricated scaffolds in this study were incorporated with these AuNPs having the aforementioned properties and their extracts in complete cell culture medium were not cytotoxic to fibroblasts and keratinocytes.

A similar strategy of incorporating AuNPs into tissue scaffolds such as decellularized porcine diaphragm (Cozad et al., 2011), collagen gel (Grant et al, 2014), polyethylene terephthalate mesh (Whelove et al., 2011), and polypropylene mesh (Grant et al., 2011) was adopted for enhanced cell attachment and/or proliferation. To generalize these studies, a specific amount of AuNPs was observed to enhance cell attachment and/or proliferation on tissue scaffolds. Like the collagen nanofibrous matrices developed in our study, AuNPs were also incorporated into nanofibrous structures made up of different materials such as poly L-lactide (McKeon-Fischer and Freeman, 2011), polyvinyl alcohol (Manjumeena et al., 2015) and polymethylglutarimide nanofibers (Jung et al., 2012). Electrospun poly (L-lactide) and AuNP (5 nm) composite scaffolds were fabricated for skeletal muscle tissue

engineering and specific amounts (7%) of AuNPs made the scaffolds biocompatible (McKeon-Fischer and Freeman, 2011). In a similar way, 0.1% loading of AuNPs (15 nm) into electrospun PVA nanofibers increased the hydrophilicity and this led to good cell adhesion and proliferation when tested for biocompatibility on Vero cell lines (Manjumeena et al., 2015). It was reported that loading AuNPs (15 nm) into polymethylglutarimide nanofibers enhanced HeLa cell attachment and potentiated cardiomyocyte differentiation of human pluripotent stem cells (Jung et al., 2012).

Development of collagen-based nanofibrous matrices is a very common trend in the investigations related to treatment of skin wounds. Thus, a wide variety of electrospun matrices fabricated from different types of collagen or its blends were investigated as potential skin wound treatment biomaterials. However, incorporation of AuNPs into collagen matrices has not been suggested for this purpose so far, though they have many unique properties that could be very beneficial from the perspective of skin tissue engineering such as improving effect of nanofibrous morphology, potential antibacterial and antiinflammatory effect, and easy immobilization of drugs and bioactive agents on the surface of AuNPs. Therefore, in this study, collagen/PEO nanofibrous matrices incorporated with AuNPs were developed. A green synthesis method based on the dissolution of collagen type I in weak acid (0.5 M acetic acid) was adopted. It was observed that spinnability of collagen solution without any toxic organic solvents could be achieved with AuNPs incorporation. The fabricated collagen/PEO nanofibrous matrices gained better morphology when the ratio of incorporated AuNPs increased. In particular, the nanofibrous matrix having the highest AuNP concentration (14.27 ppm) had excellent morphology. Physicochemical characterization tests indicated that AuNPs were stabilized inside the collagen fibers, and the original α-helix structure of collagen type I was maintained after processing steps. Although CM-AuX had a worse degradation profile and lower water swelling than Matriderm, it had better mechanical properties than it. The biocompatibility of the synthesized AuNPs and the extract of CM-AuX were confirmed with MTT assays. Cell attachment and proliferation results of CM-AuX were similar to those of Matriderm. Therefore, it was suggested that CM-AuX could be a very promising scaffold for skin tissue engineering.

Acknowledgment

This study was financially supported by the Scientific and Technological Research Council of Turkey (TÜBİTAK Project No: 111M810).

References

Agarwal S, Mishra P, Shivange G, Kodipelli N, Moros M, de la Fuente JM, Anindya R (2015). Citrate-capped gold nanoparticles for the label-free detection of ubiquitin C-terminal hydrolase-1. Analyst 140: 1166–1173.

Baker BM, Gee AO, Metter RB, Nathan AS, Marklein RA, Burdick JA, Mauck RL (2008). The potential to improve cell infiltration in composite fiber-aligned electrospun scaffolds by the selective removal of sacrificial fibers. Biomaterials 29: 2348–2358.

Balasubramani G, Ramkumar R, Krishnaveni N, Pazhanimuthu A, Natarajan T, Sowmiya R, Perumal P (2015). Structural characterization, antioxidant and anticancer properties of gold nanoparticles synthesized from leaf extract (decoction) of *Antigonon leptopus* Hook. & Arn. J Trace Elem Med Biol 30: 83–89.

Buttafoco L, Kolkman NG, Engbers-Buijtenhuijs P (2006). Electrospinning of collagen and elastin for tissue engineering applications. Biomaterials 27: 724–734.

Castaneda L, Valle J, Yang N, Pluskat S, Slowinska K (2008). Collagen cross-linking with Au nanoparticles. Biomacromolecules 9: 3383–3388.

Chakrapani VY, Gnanamani A (2012). Electrospinning of type I collagen and PCL nanofibers using acetic acid. J Appl Polym Sci 125: 3221–3227.

Chang MC, Tanaka J (2002). FT-IR study for hydroxyapatite/collagen nanocomposite cross-linked by glutaraldehyde. Biomaterials 23: 4811–4818.

Charulatha V, Rajaram A (2003). Influence of different cross-linking treatments on the physical properties of collagen membranes. Biomaterials 24: 759–767.

Chen JP, Chang GY, Chen JK (2008). Electrospun collagen/chitosan nanofibrous membrane as wound dressing. Colloid Surface A 313–314: 183–188.

Cozad M, Bachman S, Grant S (2011). Assessment of decellularized porcine diaphragm conjugated with gold nanomaterials as a tissue scaffold for wound healing. J Biomed Mater Res A 99: 426–434.

Cui Q, Yashchenok A, Zhang L, Li L, Masic A, Wienskol G, Möhwald H, Bargheer M (2014). Fabrication of bifunctional gold/gelatin hybrid nanocomposites and their application. ACS Appl Mater Interfaces 6: 1999–2002.

Deeken CR, Fox DB, Bachman SL, Ramshaw BJ, Grant SA (2011). Characterization of bionanocomposite scaffolds comprised of amine-functionalized gold nanoparticles and silicon carbide nanowires crosslinked to an acellular porcine tendon. J Biomed Mater Res B 97: 334–344.

Dong B, Arnoult O, Wnek GE (2009). Electrospinning of collagen nanofiber scaffolds from benign solvents. Macromol. Rapid Commun 30: 539–542.

Duan H, Feng B, Guo X, Wang J, Zhao L, Zhou G, Liu W, Cao Y, Zhang W (2013). Engineering of epidermis skin grafts using electrospun nanofibrous gelatin/polycaprolactone membranes. Int J Nanomed 8: 2077–2084.

Duan X, Sheardown H (2006). Dendrimer crosslinked collagen as a corneal tissue engineering scaffold: mechanical properties and corneal epithelial cell interactions. Biomaterials 27: 4608–4617.

Ehmann HMA, Breitwieser D, Winter S, Gspan C, Koraimann G, Maver U, Sega M, Köstler S, Stana-Kleinschek K, Spirk S et al. (2015). Gold nanoparticles in the engineering of antibacterial and anticoagulant surfaces. Carbohyd Polym 117: 34–42.

Fathi-Azarbayjani A, Qun L, Chan YW, Chan SY (2010). Novel vitamin and gold-loaded nanofiber facial mask for topical delivery. Aaps Pharmscitech 11: 1164–1170.

Fischer RL, McCoy MG, Grant SA (2012). Electrospinning collagen and hyaluronic acid nanofiber meshes. J Mater Sci-Mater M 23: 1645–1654.

Fleischer S, Shevach M, Feiner R, Dvir T (2014). Coiled fiber scaffolds embedded with gold nanoparticles improve the performance of engineered cardiac tissues. Nanoscale 6: 9410–9414.

Frens G (1973). Controlled nucleation for regulation of particle-size in monodisperse gold suspensions. Nature Physical Science 241: 20–22.

Goodman CM, McCusker CD, Yilmaz T (2004). Toxicity of gold nanoparticles functionalized with cationic and anionic side chains. Bioconjugate Chem 157: 897–900.

Gopalakrishnan R, Azhagiya Singam ER, Vijaya Sundar J, Subramanian V (2015). Interaction of collagen like peptides with gold nanosurfaces: a molecular dynamics investigation. Phys Chem Chem Phys 17: 5172–5186.

Grant DN, Benson J, Cozad MJ, Whelove OE, Bachman SL, Ramshaw BJ, Grant DA, Grant SA (2011). Conjugation of gold nanoparticles to polypropylene mesh for enhanced biocompatibility. J Mater Sci-Mater M 22: 2803–2812.

Grant SA, Spradling CS, Grant DN, Fox DB, Jimenez L, Grant DA, Rone RJ (2014). Assessment of the biocompatibility and stability of a gold nanoparticle collagen bioscaffold. J Biomed Mater Res A 102: 332–339.

Higuchi A, Tsukamoto Y (2004). Cell separation of hepatocytes and fibroblasts through surface-modified polyurethane membranes. J Biomed Mater Res A 71: 470–479.

Hsu FY, Hung YS, Liou HM, Shen CH (2010). Electrospun hyaluronate–collagen nanofibrous matrix and the effects of varying the concentration of hyaluronate on the characteristics of foreskin fibroblast cells. Acta Biomater 6: 2140–2147.

Huang GP, Shanmugasundaram S (2015). An investigation of common crosslinking agents on the stability of electrospun collagen scaffolds. J Biomed Mater Res A 103: 762–771.

Huang L, Nagapudi K, Apkarian RP (2001). Engineered collagen–PEO nanofibers and fabrics. J Biomat Sci-Polym E 12: 979–993.

Hung HS, Chang CH, Chang CJ, Tang CM, Kao WC, Lin SZ, Hsieh HH, Chu MY, Sun WS, Hsu SH (2014). In vitro study of a novel nanogold-collagen composite to enhance the mesenchymal stem cell behavior for vascular regeneration. PLoS ONE 9: e104019.

Jin HJ, Chen J, Karageorgiou V, Altman GH, Kaplan DL (2004). Human bone marrow stromal cell responses on electrospun silk fibroin mats. Biomaterials 25: 1039–1047.

Jung D, Minami I, Patel S, Lee J, Jiang B, Yuan Q, Li L, Kobayashi S, Chen Y, Lee KB et al. (2012). Incorporation of functionalized gold nanoparticles into nanofibers for enhanced attachment and differentiation of mammalian cells. J Nanobiotechnology 10: 23.

Kimling J, Maier M, Okenve B, Kotaidis V, Ballot H, Plech A (2006). Turkevich method for gold nanoparticle synthesis revisited. J Phys Chem B 110:15700–15707.

Ko WK, Heo DN, Moon HJ, Lee SJ, Bae MS, Lee JB, Sun IC, Jeon HB, Park HK, Kwon IK (2015). The effect of gold nanoparticle size on osteogenic differentiation of adipose-derived stem cells. J Colloid Interf Sci 438: 68–76.

Lee CH, Chang SH, Chen WJ, Hung KC, Lin YH (2015). Augmentation of diabetic wound healing and enhancement of collagen content using nanofibrous glucophage-loaded collagen/PLGA scaffold membranes. J Colloid Interf Sci 439: 88–97.

Li X, Robinson SM, Gupta A, Saha K, Jiang Z, Moyano DF, Sahar A, Riley MA, Rotello VM (2014). Functional gold nanoparticles as potent antimicrobial agents against multi-drug-resistant bacteria. ACS Nano 8: 10682–10686.

Lin HY, Kuo YJ, Chang SH, Ni T (2013). Characterization of electrospun nanofiber matrices made of collagen blends as potential skin substitutes. Biomed Mater 8: 025009.

Liu SJ, Kau YC, Chou CY, Chen JK, Wu RC (2010). Electrospun PLGA/collagen nanofibrous membrane as early-stage wound dressing. J Membrane Sci 355: 53–55.

Lowery JL, Datta N, Rutledge GC (2010). Effect of fiber diameter, pore size and seeding method on growth of human dermal fibroblasts in electrospun poly(epsilon-caprolactone) fibrous mats. Biomaterials 31: 491–504.

Lu S, Xia D, Huang G, Jing H, Wang Y, Gu H (2010). Concentration effect of gold nanoparticles on proliferation of keratinocytes. Colloid Surface B 81: 406–411.

Manjumeena R, Elakkiya T, Duraibabu D, Feroze Ahamed A, Kalaichelvan P, Venkatesan R (2015). "Green" biocompatible organic-inorganic hybrid electrospun nanofibers for potential biomedical applications. J Biomater Appl 29: 1039–1055.

Matthews JA, Wnek GE, Simpson DG, Bowlin GL (2002). Electrospinning of collagen nanofibers. Biomacromolecules 3: 232–238.

McKeon-Fischer KD, Freeman JW (2011). Characterization of electrospun poly(L-lactide) and gold nanoparticle composite scaffolds for skeletal muscle tissue engineering. J Tissue Eng Regen M 5: 560–568.

Obaid G, Chambrier I, Cook MJ, Russell DA (2015). Cancer targeting with biomolecules: a comparative study of photodynamic therapy efficacy using antibody or lectin conjugated phthalocyanine-PEG gold nanoparticles. Photochem Photobiol Sci 14: 737–747.

Pan Y, Neuss S, Leifert A, Fischler M, Wen F, Simon U, Schmid G, Brandau W, Jahnen-Dechent W (2007). Size-dependent cytotoxicity of gold nanoparticles. Small 3: 1941–1949.

Patra HK, Banerjee S, Chaudhuri U, Lahiri P, Dasgupta A (2007). Cell selective response to gold nanoparticles. Nanomed-Nanotechnol 3: 111–119.

Paviolo C, Chon JW, Clayton AH (2015). Inhibiting EGFR clustering and cell proliferation with gold nanoparticles. Small 11: 1638–1643.

Ravichandran R, Sridhar R, Venugopal JR, Sundarrajan S, Mukherjee S, Ramakrishna S (2014). Gold nanoparticle loaded hybrid nanofibers for cardiogenic differentiation of stem cells for infarcted myocardium regeneration. Macromol Biosci 14: 515–525.

Regiel-Futyra A, Kus-Liśkiewicz M, Sebastian V, Irusta S, Arruebo M, Stochel G, Kyzioł A (2015). Development of noncytotoxic chitosan-gold nanocomposites as efficient antibacterial materials. ACS Appl Mater Interfaces 7: 1087–1099.

Rho KS, Jeong L, Lee G, Seo BM, Park YJ, Hong SD (2006). Electrospinning of collagen nanofibers: effects on the behavior of normal human keratinocytes and early-stage wound healing. Biomaterials 27: 1452–1461.

Sanna V, Pala N, Dessì G, Manconi P, Mariani A, Dedola S, Rassu M, Crosio C, Iaccarino C, Sechi M (2014). Single-step green synthesis and characterization of gold-conjugated polyphenol nanoparticles with antioxidant and biological activities. Int J Nanomed 9: 4935–4951.

Schlinkert P, Casals E, Boyles M, Tischler U, Hornig E, Tran N, Zhao J, Himly M, Riediker M, Oostingh G et al. (2015). The oxidative potential of differently charged silver and gold nanoparticles on three human lung epithelial cell types. J Nanobiotechnology 13: 1.

Shevach M, Fleischer S, Shapira A, Dvir T (2014). Gold nanoparticle-decellularized matrix hybrids for cardiac tissue engineering. Nano Lett 14: 5792–5796.

Silveira PCL, Venâncio M, Souza PS, Victor EG, de Souza Notoya F, Paganini CS, Streck EL, da Silva L, Pinho RA, Paula MMS (2014). Iontophoresis with gold nanoparticles improves mitochondrial activity and oxidative stress markers of burn wounds. Mater Sci Eng C Mater Biol Appl 44: 380–385.

Silver F (1994). Biomaterials, Medical Devices and Tissue Engineering: An Integrated Approach. 1st ed. London, UK: Chapman and Hall.

Sionkowska A, Kozłowska J (2010). Characterization of collagen/hydroxyapatite composite sponges as a potential bone substitute. Int J Biol Macromol 47: 483–487.

Wang S, Lu W, Tovmachenko O, Rai US, Yu H (2008). Challenge in understanding size and shape dependent toxicity of gold nanomaterials in human skin keratinocytes. Chem Phys Lett 463: 145–149.

Whelove OE, Cozad MJ, Lee BD, Sengupta S, Bachman SL, Ramshaw BJ, Grant SA (2011). Development and in vitro studies of a polyethylene terephthalate-gold nanoparticle scaffold for improved biocompatibility. J Biomed Mater Res B 99: 142–149.

Wittaya-Areekul S, Prahsarn C (2006). Development and in vitro evaluation of chitosan–polysaccharides composite wound dressings. Int J Pharm 313:123–128.

Zhang M, Wang J, Xu W, Luan J, Li X, Zhang Y, Dong H (2015). The mechanical property of *Rana chensinensis* skin collagen/poly (L-lactide) fibrous membrane. Mater Lett 139: 647–470.

Zhou T, Wang N, Xue Y, Ding T, Liu X, Mo X, Sun J (2015). Development of biomimetic tilapia collagen nanofibers for skin regeneration through inducing keratinocytes differentiation and collagen synthesis of dermal fibroblasts. ACS Appl Mater Interfaces 7: 3253–3262.

Zhou Y, Kong Y, Kundu S, Cirillo J, Liang H (2012). Antibacterial activities of gold and silver nanoparticles against *Escherichia coli* and bacillus Calmette-Guérin. J Nanobiotechnology 10: 19.